Bending of a Cosserat Elastic Bar of Square Cross Section - Theory and Experiment

Roderic Lakes, W. J. Drugan *†
Department of Engineering Physics, Engineering Mechanics Program,
Department of Materials Science, Rheology Research Center,
University of Wisconsin, 1500 Engineering Drive, Madison, WI 53706-1687
Preprint Journal of Applied Mechanics, 82(9), 091002 (Sep 01, 2015) (8 pages)

June 30, 2015

Abstract

Pure bending experiments on prismatic bars of square cross-section composed of reticulated polymer foam exhibit deformation behavior not captured by classical elasticity theory. Perhaps the clearest example of this is the observed sigmoidal deformation of the bars' lateral surfaces, which are predicted by classical elasticity theory to tilt but remain planar upon pure moment application. Such foams have a non-negligible length scale compared to the bars' cross-section dimensions, whereas classical elasticity theory contains no inherent length scale. All these facts raise the intriguing question: is there a richer, physically-sensible, yet still continuum and relatively simple elasticity theory capable of modeling the observed phenomenon in these materials? This paper reports our exploration of the hypothesis that Cosserat elasticity can. We employ the principle of minimum potential energy for homogeneous isotropic Cosserat elastic material in which the microrotation vector is taken to be independent of the macrorotation vector (as prior experiments indicate it should be in general to model such materials) to obtain an approximate three-dimensional solution to pure bending of a prismatic bar having a square cross-section. We show that this solution, and hence Cosserat elasticity, captures the experimentally-observed nonclassical deformation feature, both qualitatively and quantitatively, for reasonable values of the Cosserat moduli. A further interesting conclusion is that a single experiment – the pure bending one – suffices to reveal directly, via the observation of surface deformation, the presence of nonclassical elastic effects describable by Cosserat elasticity.

*lakes@engr.wisc.edu
†drugan@engr.wisc.edu

1 Introduction

For many purposes it is expedient to make use of continuum representations of materials, all of which actually have microstructure. Several such continuum theories with different amounts of freedom are available. An early theory of Navier called uniconstant was proposed based on atomic interaction theory. It had too little freedom and was abandoned since it predicted a Poisson's ratio of 1/4 for all materials. The elasticity theory currently accepted as classical allows Poisson's ratios in isotropic materials in the range -1 to $1/2$. Translations of points are allowed but not point rotations. Classical elasticity has no length scale. By contrast, Cosserat elasticity allows rotations of points and has a length scale, so it is pertinent to the deformation of heterogeneous materials whose heterogeneity size scale is not negligible compared to dimensions of a structural component or the sizes of e.g. holes or cracks, or the length scale of the phenomenon under investigation, such as wavelength in a wave propagation problem. Too, the toughness of materials has a length scale; the value of this length cannot be extracted from the classical elastic properties of the material. The toughness of foams is calculated by considering a crack in the foam under tension, and analyzing the bending of the cell ribs [1]; the toughness depends on the cell size in the foam.

The constitutive equations for an isotropic Cosserat [2] or micropolar [3] elastic solid are

$$\sigma_{ij} = 2G\epsilon_{ij} + \lambda\epsilon_{kk}\delta_{ij} + \kappa e_{ijk}(r_k - \phi_k) \tag{1}$$

$$m_{ij} = \alpha\phi_{k,k}\delta_{ij} + \beta\phi_{i,j} + \gamma\phi_{j,i} \tag{2}$$

in which σ_{ij} is the force stress tensor (symmetric in classical elasticity but asymmetric here), m_{ij} is the couple stress tensor (moment per unit area, asymmetric in general), $\epsilon_{ij} = (u_{i,j} + u_{j,i})/2$ is the small strain tensor, u_i the displacement vector, and e_{ijk} is the permutation symbol. The microrotation vector ϕ_i in Cosserat elasticity is kinematically distinct from the macrorotation vector $r_i = (e_{ijk}u_{k,j})/2$. ϕ_i refers to the rotation of points themselves, while r_i refers to the rotation associated with movement of nearby points. The usual Einstein summation convention for repeated indices is employed, and a comma denotes differentiation with respect to ensuing subscripts which represent spatial Cartesian coordinates.

Some authors, e.g. [4], object to the notion of an independent microrotation vector. If one assumes, following Koiter [5] (who did so for simplicity), that the macrorotation and microrotation vectors are equal, then in Cosserat elasticity, N = 1, or equivalently $\kappa \to \infty$ [see Eq. (8)]. Careful size effect experiments, however, give measured N values that are significantly smaller than unity [6, 7]. Furthermore, the notion of independent microrotation is confirmed theoretically in homogenization analyses for various lattices and composites; see e.g. [8] and several references cited therein. Although prior experiments exclude N = 1 for foams and bone, they do not necessarily exclude the presence of additional freedom such as that incorporated in micromorphic / Mindlin microstructure theory.

As Eqns. (1, 2) show, six independent elastic constants are required to describe general three-dimensional deformations of an isotropic Cosserat elastic solid: α, β, γ, κ, λ, and G. (Eringen [3] uses $2\mu + \kappa = 2G$, so μ differs from the shear modulus G in his notation.) Classical elasticity is a special case, achieved by allowing α, β, γ, κ to become zero. The classical Lamé elastic constants

λ and G then remain, and there is no couple stress. Technical constants are as follows:

$$Young's\ modulus \qquad E = \frac{(2G)(3\lambda + 2G)}{2\lambda + 2G} \tag{3}$$

$$Shear\ modulus \qquad G \tag{4}$$

$$Poisson's\ ratio \qquad \nu = \frac{\lambda}{2(\lambda + G)} \tag{5}$$

$$Characteristic\ length,\ torsion \qquad \ell_t = \sqrt{\frac{\beta + \gamma}{2G}} \tag{6}$$

$$Characteristic\ length,\ bending \qquad \ell_b = \sqrt{\frac{\gamma}{4G}} \tag{7}$$

$$Coupling\ number \qquad N = \sqrt{\frac{\kappa}{2G + \kappa}} \tag{8}$$

$$Polar\ ratio \qquad \Psi = \frac{\beta + \gamma}{\alpha + \beta + \gamma}. \tag{9}$$

Continuum theories make no reference to structural features; however, they are intended to represent physical solids which always have some form of microstructure. The couple stresses in Cosserat and microstructure elasticity represent spatial averages of distributed moments per unit area, just as the ordinary (force) stress represents a spatial average of force per unit area. While such moments can occur on the atomic scale or the nano scale, moments may be also transmitted on a much larger scale, through fibers in fiber-reinforced materials or in the cell ribs or walls in cellular solids. The Cosserat characteristic lengths will then be associated with the physical size scales in the microstructure, and be sufficiently large to observe experimentally on the micro-scale or the milli-scale.

Structures of sufficient regularity can be subject to homogenization analysis to extract the elastic constants, including Cosserat constants. In lattice type cellular solids the characteristic length may be comparable to the average cell size [9]. Bigoni and Drugan [10] derived homogeneous Cosserat material moduli that best represent heterogeneous Cauchy material behavior under general loading. They applied this to two specific matrix-inclusion composite microstructures: one with cylindrical inclusions (2D plane strain), and one with spherical inclusions (3D). They showed the Cosserat characteristic length can be determined analytically when inclusions are less stiff than the matrix, but when these are equal to or stiffer than the matrix, Cosserat effects were shown to be excluded.

Cosserat elastic effects have been observed experimentally. For example, size effects are observed to occur in torsion and bending of foams [6, 7] and of compact bone. Size effect in bone exceeds a factor of three in effective shear modulus [11]. Classical elasticity predicts effective shear modulus independent of specimen size. Experiments show the apparent modulus increases substantially as the specimen diameter becomes smaller. The Cosserat continuum concept accounts for these observations. From a micro-structural perspective, a contribution to the twisting or bending moment arises from twist or bend of each individual fiber in fibrous materials or each rib in cellular solids, hence size effects. Heterogeneous structure does not necessarily give rise to size effects: no size effects were observed in particulate composites with large particles [12] nor in syntactic foams that contain small particles [6], and as mentioned Bigoni and Drugan [10] showed theoretically that no Cosserat effects occur for inclusions stiffer than the matrix (for cylindrical inclusions in plane strain, and for spherical inclusions in 3D). The Cosserat characteristic length was determined in a polymer honeycomb as a two dimensional system [13]. On smaller scales, asymmetric interatomic action was studied in magnetic media; the existence of non-central load was demonstrated with

electron paramagnetic resonance [14].

Experiments are interpreted with the aid of analytical solutions for the configuration under study. For example, analytical solutions are known for torsion [12] and bending [15] of an isotropic Cosserat linear elastic circular cylinder. These analyses disclose size effects in structural rigidity in which slender rods are stiffer than predicted by classical elasticity using moduli obtained in the absence of gradients.

Changes in the surface deformation field are of particular interest in experiments. For example, a bar of rectangular cross section in torsion exhibits warp, an in-plane deformation parallel to the surface. The classical warp is predicted to be reduced in a Cosserat elastic solid [16]; this gives rise to an observed redistribution of strain away from regions that are classically highly strained [17] [18] into classically low strain regions. This ameliorates concentration of strain. The reduction of warp has been observed via holography [19].

Bending of Cosserat elastic bars of non-circular cross section is of interest in the context of change in deformation field. Saint Venant's problem has been considered in an abstract sense that shows existence of solution [20]; bending has been considered in terms of functions to be determined [21]. A plane stress approximation for $\kappa \to \infty$ was presented, showing changes in stress fields [22], hence size effects. Plate bending also discloses size effects in the rigidity [12]. Several beam theory analyses have been presented [23]; cross section shape change was not considered. A three dimensional analysis was presented [24] in which constraints on the lateral deformation were imposed. In summary, none of the available studies of bending deals with deformations of a prismatic bar of square cross section subjected to pure bending.

Previous experiments on two foam types have provided the following values for the isotropic classical and Cosserat elastic moduli (via the technical constants of Eqs. (3-9)): For dense polyurethane foam [6], $E = 300$ MPa, $G = 104$ MPa, $\nu = 0.4$, $\ell_t = 0.62$ mm, $\ell_b = 0.33$ mm, $N^2 = 0.04$, $\Psi = 1.5$. This is a closed cell foam of density 340 kg/m^3; the cell size is 0.05 to 0.15 mm.

For polymethacrylamide closed cell foam type Rohacell WF300 [7], $E = 637$ MPa, $G = 285$ MPa, $\ell_t = 0.8$ mm, $\ell_b = 0.77$ mm, $N^2 \approx 0.04$, $\Psi = 1.5$. This is a closed cell foam of density 380 kg/m^3; the cell size is 0.65 mm. Inference of Poisson's ratio from Young's and shear modulus gives $\nu = 0.12$; the low value is likely due to slight anisotropy in the foam. Other polymethacrylamide foams studied in this series had density 110 kg/m^3 and 60 kg/m^3; characteristic lengths were somewhat smaller; N was not accurately determined owing to the difficulty in cutting sufficiently slender specimens.

Thus, in these previously-tested foams, ℓ_b ranged between approximately 1.2 to 6.6 times the cell size. As noted, these were closed-cell foams, in contrast to the open-cell foams tested in the present work.

The present research explores bending of a bar of square cross section in which Cosserat effects give rise to out of plane effects normal to the surface. Such effects are particularly amenable to experiment.

2 Experiment

2.1 Materials and methods

Bars of open cell reticulated polyurethane foam (Scott Industrial foam [25]) were used. They were 50 mm in square cross section and about 300 mm long. One foam had average cell size 1.2 mm or 20 pores per inch (Figure 1); the other foam had average cell size 0.4 mm (Figure 2). The mass and dimensions of each bar were measured. Flat stalks about 30 cm long were cemented to each end. Displacement of the surface was measured via digital photography. Shadow Moiré was attempted

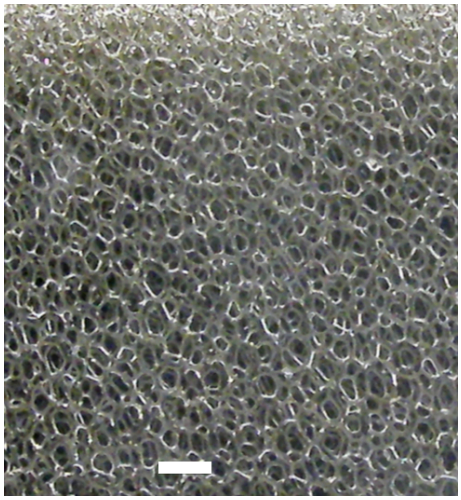

Figure 1: Open cell polyurethane foam. Scale bar, 5 mm.

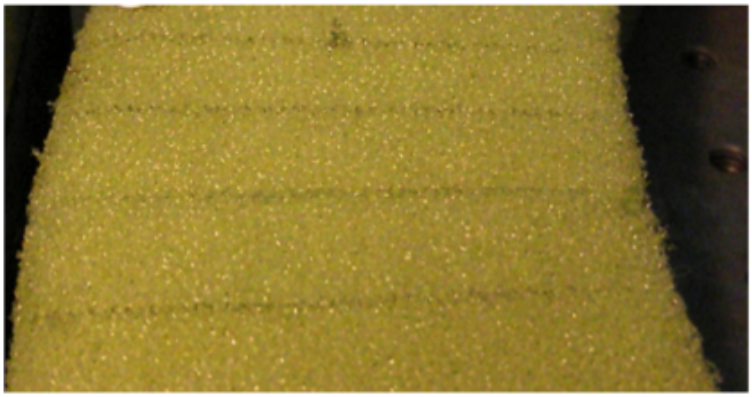

Figure 2: Portion of the bent 50 mm wide test beam of 0.4 mm cell size foam viewed at an oblique angle.

but surface roughness and light penetration precluded useful fringes. The foam bar was placed on an optical table and a digital camera was mounted at an oblique angle above it. Fiducial cross section lines were drawn on the foam with ink or acrylic paint. Pure bending was achieved by bringing the ends of the stalks into contact. The stalk length defined the radius of curvature $R = 27.5$ cm from the neutral axis. Sigmoid bulge was sufficient to be discerned by the unaided eye. The maximum strain was 4.5%, within the linear range for this class of foam. Digital photographs were taken before and after bending. A thin straight line was drawn digitally on each image from corresponding points at the edges. These points were used as reference points corresponding to zero motion; this procedure eliminates the effect of classical tilt. Displacements were measured on the images via GIMP image processing software. No averaging or smoothing was done. Pixel count was converted to displacement using the known width of the bar; the scale factor was about 30 pixels per millimeter. Because the end points correspond to zero motion, the tilt deformation of the lateral surfaces is subtracted out. Several such experiments were done. Curve fits of sinusoidal form serve as guides to the eye. Tilt deformation was evaluated via photographs taken from an

orthogonal direction.

Tests were also done to probe anisotropy. Cubes of foam were cut and compressed to less than 5% strain in a servo-hydraulic frame. Compression was done in each of three orthogonal directions to determine moduli.

2.2 Results

Results are shown in Figure 3. The lateral surface exhibits a sigmoid bulge deformation in which the magnitude is larger for the larger cell foam. Scatter in the points arises from heterogeneity in the deformation of the foam cells. The density of each foam was $\rho = 0.030$ g/cm^3 or 30 kg/m^3. Tilt deformation is not shown in the graphs because the image processing method defines the motion at the edges (i.e., corners) to be zero. Scatter of the points is attributed largely to the non-affine deformation known to occur in foams. Pixel resolution also contributes to the scatter for the smaller cell foam.

The foam with 1.2 mm cells had a ratio of moduli in different directions of 1.6, indicating substantial anisotropy; the foam with 0.4 mm cells was isotropic to within 10%.

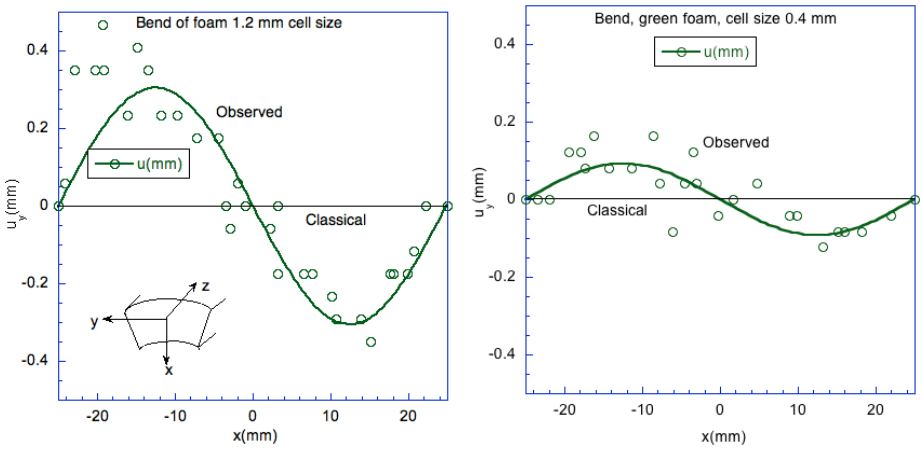

Figure 3: Deformation u_y vs. position, excluding tilt; left, larger cell foam, cell size 1.2 mm; right, cell size 0.4 mm. Comparison of the two figures shows the sigmoidal displacement is increased for larger pore size, implying a local length scale effect that suggests modeling via Cosserat theory.

3 Bending analysis

3.1 Three-dimensional governing equations for a Cosserat medium

The complete governing equations for three-dimensional infinitesimal deformations of a homogeneous, isotropic linear elastic Cosserat medium in equilibrium with no body forces are the constitutive equations (1) and (2), the strain-displacement and macrorotation-displacement equations noted earlier, namely

$$\epsilon_{ij} = (u_{i,j} + u_{j,i})/2 \tag{10}$$

$$r_i = (e_{ijk} u_{k,j})/2, \tag{11}$$

and the equations of force and moment equilibrium, respectively

$$\sigma_{ij,i} = 0 \tag{12}$$

$$m_{ij,i} + e_{jkl}\sigma_{kl} = 0. \tag{13}$$

For all boundary portions on which displacements are not prescribed, the force traction vector t_i and the moment traction vector m_i must be prescribed; these are related through the boundary's outward unit normal vector n_i to the force and couple stress tensors as

$$t_i = \sigma_{ji}n_j, \quad m_i = m_{ji}n_j. \tag{14}$$

3.2 Classical three-dimensional pure bending solution

The classical three-dimensional displacement field solution for pure bending of prismatic bars in homogeneous, isotropic linear elasticity is

$$u_x = -\frac{z^2 + \nu(x^2 - y^2)}{2R}, \quad u_y = -\nu\frac{xy}{R}, \quad u_z = \frac{xz}{R}, \tag{15}$$

where R is the principal radius of curvature of bending (produced by pure moments about the y-axis in Figure 4). Substitution of Eqs. (15) into Eq. (10) gives the strain field

$$\epsilon_{xx} = \epsilon_{yy} = -\nu\frac{x}{R}, \quad \epsilon_{zz} = \frac{x}{R}, \quad \text{all other} \quad \epsilon_{ij} = 0. \tag{16}$$

When the Cosserat moduli α, β, γ, κ are all zero, substitution of Eqs. (16) into (1) gives the stress field

$$\sigma_{zz} = 2G(1+\nu)\frac{x}{R}, \quad \text{all other} \quad \sigma_{ij} = 0. \tag{17}$$

This clearly satisfies the equilibrium equations (12) and zero force traction vector on all beam surfaces except the ends; thus, as is well known, the stress distribution (17) and its associated displacement (15) and strain (16) fields is an exact three-dimensional classical elasticity solution for pure bending of a prismatic bar when the pure bending moments are applied to the bar ends by a normal stress distribution given by σ_{zz} in (17).

In the classical displacement field solution of Eq. (15), applied to a bar of square cross-section as considered here, dependence on ν in u_x represents the anticlastic curvature of bending, while displacement u_y represents tilt of lateral surfaces due to the Poisson effect. We emphasize that the displacement component u_y exhibits purely a linear dependence on x, meaning that the originally vertical sides of the beam tilt, but remain planar - see Figure 4. However, the experimental measurements reported in Figure 3 clearly show that the foam beam sides deform to a non-planar shape. We now investigate whether Cosserat elasticity is able to capture this deformation feature not exhibited by classical elasticity.

3.3 Can the classical bending solution also solve Cosserat bending?

As just reviewed, (15) is an exact three-dimensional solution to the classical elasticity governing equations and boundary conditions for pure bending of a prismatic bar. We wish to find the three-dimensional displacement field solution for pure bending of a square-cross-section bar composed of Cosserat elastic material. We first explore, following Koiter [5], the degree to which the classical displacement field (15) can be a solution; we begin by temporarily making the simplifying assump-

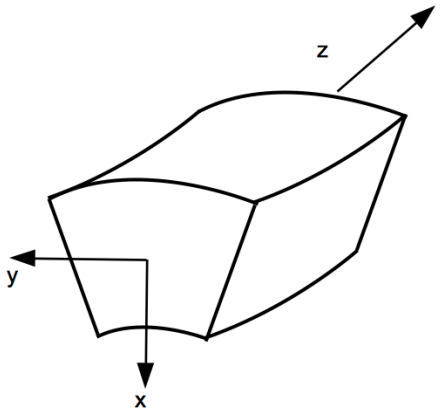

Figure 4: Deformed shape of a bar of initially square cross-section experiencing pure bending by moments at ends acting in the positive-y direction, showing anticlastic curvature and tilt of lateral surfaces.

tion he made: that the Cosserat microrotation $\phi_i = r_i$. (This equality is forced if $\frac{\kappa}{G} \to \infty$.) This assumption means, using (15) in (11), that

$$\phi_x = 0, \quad \phi_y = -z/R, \quad \phi_z = -\nu y/R. \tag{18}$$

The strain field (16) is unchanged; when it and $\phi_i = r_i$ are substituted into (1) with nonzero Cosserat moduli, and (18) are substituted into (2), we obtain the following Cosserat force and couple stress fields, respectively:

$$\sigma_{zz} = 2G(1+\nu)\frac{x}{R}, \quad \text{all other} \quad \sigma_{ij} = 0. \tag{19}$$

$$m_{yz} = -\frac{\beta+\gamma\nu}{R}, \quad m_{zy} = -\frac{\beta\nu+\gamma}{R}, \quad \text{all other} \quad m_{ij} = 0. \tag{20}$$

These fields exactly satisfy all the equilibrium field equations (12, 13). If on the beam ends the force and couple traction vectors are applied in accord with (14, 19, 20), the boundary conditions are exactly satisfied everywhere, except for the requirement of zero applied m_{yz} on the beam's $y =$ constant lateral surfaces. Eqs. (20) show this latter requirement can be met exactly only if $\beta/\gamma = -\nu$. If $\beta/\gamma \neq -\nu$, the above solution is exact only if a uniform m_{yz}, equal to that given in Eqs. (20), is applied everywhere on the beam's $y =$ constant lateral surfaces. Thus, when the beam's lateral surfaces are force and moment traction-free, as in the experiments described above, and the material's $\beta/\gamma \neq -\nu$, the deformation field must be non-classical.

Size effects are predicted by calculating the total moment acting on the beam ends due to the force stress and couple stress distributions. As a simple illustration, for the case $\beta/\gamma = -\nu$, the above solution is an exact Cosserat one as noted. Eqs. (20) then show that $m_{zy} \neq 0$, so it contributes to the total moment along with σ_{zz}, giving the result (I is the area moment of inertia):

$$M = \frac{EI}{R}[1 + 24(\frac{\ell_b}{2a})^2(1-\nu)]. \tag{21}$$

3.4 Approximate three-dimensional Cosserat bending solution

As an exact closed-form three-dimensional Cosserat bending solution does not appear to be possible (except if $\beta/\gamma = -\nu$ as just noted), we derive a simple approximate solution. This is accomplished by deriving the correction to the classical displacement field solution of Eqs. (15) and associated micro-rotation field of Eqs. (18) needed to remove the m_{yz} distribution on the $y =$ constant lateral beam surfaces. The approximate three-dimensional Cosserat solution is then the superposition of Eqs. (15, 18) and the correction fields derived next.

We now analyze the correction problem of a beam of square cross-section of side length $2a$ (lying in the x, y-plane of Figure 4) having force- and moment-traction-free sides except that

$$m_{yz} = \frac{\beta + \gamma\nu}{R} \quad \text{on} \quad y = \pm a. \tag{22}$$

Our approach is to employ polynomial representations for the displacement and Cosserat microrotation components that will be nonzero in this correction problem, employing polynomials of just sufficiently high order that they will be capable of representing the nonlinear antisymmetric lateral beam side distortions exhibited by the experiments. Specifically, we seek an approximate solution of the form, with the constants a_i, b_i, c_i being initially undetermined and rigid-body motion excluded:

$$\begin{aligned}
u_x &= a_1x^2 + a_2xy + a_3y^2 + a_4x^3 + a_5x^2y + a_6xy^2 + a_7y^3 + a_8x^4 + a_9x^3y + a_{10}x^2y^2 + a_{11}xy^3 + a_{12}y^4 \\
u_y &= b_1x^2 + b_2xy + b_3y^2 + b_4x^3 + b_5x^2y + b_6xy^2 + b_7y^3 + b_8x^4 + b_9x^3y + b_{10}x^2y^2 + b_{11}xy^3 + b_{12}y^4 \\
\phi_z &= c_1x + c_2y + c_3x^2 + c_4xy + c_5y^2 + c_6x^3 + c_7x^2y + c_8xy^2 + c_9y^3 \\
u_z &= \phi_x = \phi_y = 0.
\end{aligned} \tag{23}$$

We determine the best possible solution of the form given in Eqs. (23) by employing the principle of minimum potential energy. For a general three-dimensional body of homogeneous, isotropic, linear elastic Cosserat material contained in volume V having surface S, the total potential energy is given by

$$\Pi = \int_V W dV - \int_S (t_i u_i + m_i \phi_i) dS, \tag{24}$$

where

$$W = G\epsilon_{ij}\epsilon_{ij} + \frac{\lambda}{2}(\epsilon_{kk})^2 + \kappa(r_i - \phi_i)(r_i - \phi_i) + \frac{1}{2}\big[\alpha(\phi_{k,k})^2 + \beta\phi_{i,j}\phi_{j,i} + \gamma\phi_{i,j}\phi_{i,j}\big]. \tag{25}$$

This is applied to the correction problem described. The fields produced by our assumed solution form, Eqs. (23), make the integrand of the surface integral in Eq. (24) zero on the bar ends, and all the fields in Eqs. (23) are independent of z, so in Eq. (24) the volume integral becomes an in-plane area integral and the surface integral an in-plane line integral with S now referring to the lateral surface of the bar. The lateral surface boundary conditions require $t_i = 0$ and $m_i = 0$ everywhere on S except, in accord with Eqs. (14, 22), $m_z = \pm(\beta + \gamma\nu)/R$ on $y = \pm a$, respectively. Using these prescribed tractions, Eqs. (23), using Eq. (11), are substituted into Eq. (24) with Eq. (25), the integrations in Eq. (24) are carried out, and the resulting total potential energy is minimized with respect to all the constants appearing in Eqs. (23). This procedure shows that most of those constants are zero (and thereby shows the symmetries and antisymmetries of the displacement and micro rotation components); renaming the surviving constants, the nonzero members of Eqs.(23) reduce to the following (where $1/a^2$ is introduced as indicated so all constants have the same

dimensions and their resulting solutions are simplified):

$$u_x = a_1 x^2 + a_2 y^2 + \frac{1}{a^2}\left(a_3 x^4 + a_4 x^2 y^2 + a_5 y^4\right) \tag{26a}$$

$$u_y = b_1 xy + \frac{1}{a^2}\left(b_2 x^3 y + b_3 x y^3\right) \tag{26b}$$

$$\phi_z = c_1 y + \frac{1}{a^2}\left(c_2 x^2 y + c_3 y^3\right). \tag{26c}$$

We now employ the following substitutions, obtained from Eqs.(5, 7, 8):

$$\lambda = \frac{2G\nu}{1-2\nu}, \quad \gamma = 4G\ell_b^2, \quad \kappa = \frac{2GN^2}{1-N^2}. \tag{27}$$

The values of the constants in Eqns. (26) from the potential energy minimization then depend only on $\nu,\ \ell_b,\ N,\ \beta/\gamma,\ a$ and R:

$$
\begin{aligned}
a_1 &= d\Big\{ N^4\left(7-19\nu+18\nu^2\right) + (\ell_b/a)^2N^2\big[371-1294\nu+1052\nu^2 \\
&\quad - 6N^2\left(35+44\nu-156\nu^2+98\nu^3\right)\big] + 18(\ell_b/a)^4\big[245-952\nu+728\nu^2 \\
&\quad - 12N^4\left(7-4\nu-31\nu^2+28\nu^3\right) - 4N^2\left(112+81\nu-486\nu^2+266\nu^3\right)\big]\Big\} \\
a_2 &= -a_1\frac{4-3\nu+\nu^2}{\nu^2} + 2a_3\frac{44-109\nu+56\nu^2}{7\nu^2} - a_4\frac{4+13\nu-8\nu^2}{3\nu^2} \\
a_3 &= \frac{7}{6}\frac{[3a_1+(1+\nu)a_4][(a/\ell_b)^2/18+1/N^2-1]-\nu a_4}{3+[1/N^2+(a/\ell_b)^2/18](4-7\nu)} \\
a_4 &= -21d\Big\{ N^4(1-\nu)^2 + (\ell_b/a)^2N^2\big[53-147\nu+88\nu^2 - 6N^2\left(5-9\nu+4\nu^2\right)\big] \\
&\quad + 18(\ell_b/a)^4\big[35-111\nu+70\nu^2 - 12N^4\left(1-3\nu+2\nu^2\right) - 2N^2\left(32-64\nu+29\nu^2\right)\big]\Big\} \\
a_5 &= a_1\frac{19-3\nu}{6\nu^2} - a_3\frac{209-565\nu+287\nu^2}{21\nu^2} + a_4\frac{19+73\nu-44\nu^2}{18\nu^2} \\
b_1 &= a_1\frac{1-4\nu+2\nu^2}{\nu^2} - (1-2\nu)\left(2a_3\frac{11-14\nu}{7\nu^2} - a_4\frac{1+2\nu}{3\nu^2}\right) \\
b_2 &= -4\frac{1-\nu}{\nu}a_3 \\
b_3 &= -\frac{2(1-\nu)}{3\nu}(3a_1+a_4) - b_1 \\
c_1 &= -\frac{6a_2+3(b_1+b_2)\left(1-2N^2\right)+2\left(a_4+c_2N^2\right)}{6N^2} \\
c_2 &= \frac{3b_2/2-a_4}{1+18(\ell_b/a)^2(1/N^2-1)} \\
c_3 &= b_3 - \frac{4a_5+b_3}{2N^2}
\end{aligned}
\tag{28}
$$

where

$$
\begin{aligned}
d = \frac{15(\ell_b/a)^2N^2(\beta/\gamma+\nu)}{4R}\Big/\Big\{ & N^6(22-19\nu) + 3(\ell_b/a)^2N^4\big[462-399\nu+N^2\left(301-612\nu+290\nu^2\right)\big] \\
& + 270(\ell_b/a)^6\big[12N^6(1-\nu)^2(5-14\nu) + 7(22-19\nu) + N^2\left(767-1522\nu+728\nu^2\right) \\
& + 4N^4\left(139-438\nu+432\nu^2-133\nu^3\right)\big] + 3(\ell_b/a)^4N^2\big[305(22-19\nu) \\
& + 3N^2\left(4439-9172\nu+4435\nu^2\right) + 6N^4\left(407-1357\nu+1195\nu^2-245\nu^3\right)\big]\Big\}.
\end{aligned}
$$

Observe that the b_2 term in Eqns. (26) represents the sigmoid bulge. The magnitude of the bulge effect is governed by $d \propto (\frac{\beta}{\gamma}+\nu)$, as expected. If $\ell_b << a$, then $d \propto (\frac{\ell_b}{a})^2$; see Eqns. (30) below.

As these expressions for the constants simplify substantially for a specific ν value, we present their reduced forms for the case $\nu = 0.3$, which applies to the 0.4 mm cell size foam tested (the c_i

expressions are unchanged and thus are not repeated):

$$
\begin{aligned}
a_1 &= \frac{d}{250}\left[730N^4 + (\ell_b/a)^2N^2(19370 - 55209N^2) + 36(\ell_b/a)^4(3115 - 49871N^2 - 5649N^4)\right] \\
a_2 &= -(6699a_1 - 9804a_3 + 5026a_4)/189 \\
a_3 &= \frac{7}{6}\frac{[30a_1 + 13a_4][(a/\ell_b)^2/18 + 1/N^2 - 1] - 3a_4}{30 + 19[1/N^2 + (a/\ell_b)^2/18]} \\
a_4 &= -\frac{21d}{100}\left[49N^4 + 2(\ell_b/a)^2N^2(841 - 798N^2) + 36(\ell_b/a)^4(400 - 1541N^2 - 168N^4)\right] \\
a_5 &= (19005a_1 - 19599a_3 + 12929a_4)/567 \\
b_1 &= -\frac{2}{189}(21a_1 + 816a_3 - 224a_4) \\
b_2 &= -\frac{28}{3}a_3 \\
b_3 &= -\frac{14}{9}(3a_1 + a_4) - b_1
\end{aligned}
\tag{29}
$$

where

$$
\begin{aligned}
d = \frac{75(\ell_b/a)^2N^2(3 + 10\beta/\gamma)}{2R}\Big/\Big[&1630N^6 + 108(\ell_b/a)^6(28525 + 93980N^2 + 42889N^4 + 1176N^6) \\
&+ 3(\ell_b/a)^4N^2(497150 + 625965N^2 + 60501N^4) + 210(\ell_b/a)^2N^4(489 + 205N^2)\Big].
\end{aligned}
$$

The case $\frac{\ell_b}{a} << 1$ also permits substantial simplification in that higher-order terms in $\frac{\ell_b}{a}$ are then negligible, but the quality of such an approximation depends on N. For the value $N = 0.62$ used in the next section, to keep truncation error below about 5%, it is necessary to have $\frac{\ell_b}{a} < 0.01$. The specimens in this study were not sufficiently thick to use such a simplification, so we have employed Eqs. (29) in our upcoming comparison with the experiments.

Nevertheless, when $\frac{\ell_b}{a}$ is sufficiently small that higher-order terms in $\frac{\ell_b}{a}$ are truly negligible, the expressions for the constants in Eqs. (28) simplify so substantially, for arbitrary ν, that we present their simplifications below. These are provided with the caution that one must ensure from the full forms in Eqs. (28) that, for the given material's N value, $\frac{\ell_b}{a}$ is indeed sufficiently small that its higher-order terms are negligible. Observe that all expressions to follow are accurate to $O[(\ell_b/a)^2]$

except that for b_1, which for similar accuracy has terms through $O[(\ell_b/a)^4]$ retained:

$$a_1 = d\big(7 - 19\nu + 18\nu^2\big), \quad a_2 = d\big(25 - \nu - 18\nu^2\big), \quad a_3 = -\frac{7}{2}d\nu(3-\nu)$$

$$a_4 = -21d(1-\nu)^2, \quad a_5 = -\frac{7}{6}d\big(44 - 35\nu - 3\nu^2\big)$$

$$b_1 = 2d\Bigg\{(1-\nu)(5-18\nu) + \left(\frac{\ell_b}{a}\right)^2\left[\frac{1}{N^2}\left(258 - 197\nu - 82\nu^2\right) + \frac{3(1-\nu)}{22-19\nu}\left(3203 - 1836\nu - 2758\nu^2 + 1496\nu^3\right)\right]\Bigg\} \tag{30}$$

$$b_2 = 14d(3-\nu)(1-\nu), \quad b_3 = 14d\nu(1-\nu), \quad c_1 = -\frac{2d}{N^2}\big[22 - 19\nu - 6N^2(1-\nu)(2-3\nu)\big]$$

$$c_2 = 42d(2-\nu)(1-\nu), \quad c_3 = \frac{14d}{3N^2}\big[22 - 19\nu + 3N^2\nu(1-\nu)\big]$$

where

$$d = \frac{15}{4}\frac{\beta/\gamma + \nu}{22 - 19\nu}\frac{(\ell_b/a)^2}{R}.$$

3.5 Comparison of Approximate Cosserat Solution with Experimental Measurements

To compare the approximate solution obtained in the previous subsection with the experimental measurements, we employ the following values corresponding to the foam bars tested:

$$a = 25\text{mm}, \quad R = 27.5\text{cm}. \tag{31}$$

Because the foam with the 1.2 mm cells is anisotropic (modulus ratio about 1.6), and the approximate solution is for an isotropic Cosserat material, we compare our results with the measurements on the foam with the 0.4 mm cell size. The Poisson's ratio of this foam was measured previously [26] to be approximately 0.3, the value also given by [1] as the mean of many measurements by various authors. We choose $\beta/\gamma = 1$ based on the results of [27], who performed homogenization analysis of a 3-D cubic lattice. If one tunes the rigidity of diagonal members in their lattice to obtain elastic isotropy, then $\frac{\beta}{\gamma} \to 1$. No Cosserat model was available for foam. The approximate analytical solution does show that one must have $\beta/\gamma > 0$ to produce the same bulge sign as observed in the experiments. The solution also shows that the bulge displacement magnitude increases with increasing β/γ (whose maximum permissible value is 1).

With a, R, ν and β/γ so specified, the displacement field approximate solution contains only the unknowns ℓ_b and N. These are obtained by matching the analytical displacement field with the experimental measurements for the smallest possible ℓ_b. The values thus obtained are

$$\ell_b = 4.5\text{mm}, \quad N^2 = 0.39. \tag{32}$$

These values have been used in the plot of our approximate analytical solution for u_y shown in Figure 5 where, as was done in the presentation of the experimental data, we have plotted the full u_y with the tilt (linear) portion removed in such a way that the displacement at the cross-section corners vanishes. Observe the qualitative, as well as quantitative, agreement with the experimental measurements reported in the right plot of Figure 3.

A single bending experiment cannot determine all Cosserat moduli. Our goal in this theory-

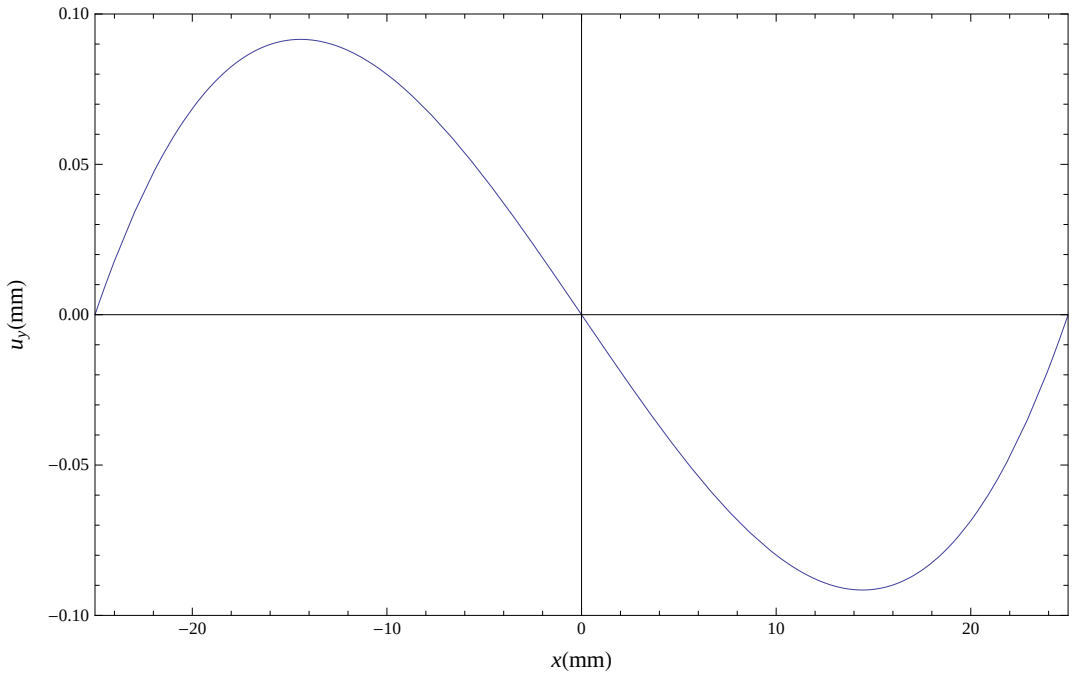

Figure 5: Approximate Cosserat analytical solution for lateral side displacement u_y (with tilt portion removed) vs. position for foam with 0.4 mm cell size.

experiment comparison is to show that an approximate Cosserat solution exhibits the experimentally-observed behavior not captured by classical elasticity, for reasonable values of the Cosserat moduli.

4 Discussion

Analysis and experiment both reveal that pure bending of a Cosserat elastic bar gives rise to a non-classical deformation field in which the lateral surfaces exhibit sigmoid bulge superposed on tilt. Full field bending deformation of a square cross section bar reveals the presence of Cosserat elasticity via observation of a single specimen. This is simpler than the size effect approach which entails rigidity measurements of a series of rods of different diameter. Size effects, if measured in both torsion and bending, allow determination of all six constants, but the method is painstaking. Observation of sigmoid bulge in bending also reveals the sign of β/γ in a simple manner from a single specimen.

Analysis also shows via b_1 in Eqns. (26) that there is a size dependent contribution to tilt of the lateral surfaces and via the a_n coefficients that there is a size dependent contribution to the anticlastic curvature. Therefore, if the characteristic length is not negligibly small, it is better to measure Poisson's ratio in tension or compression rather than in bending, as was done by [26] for the 0.4 mm cell size foam.

Generalized continuum theories such as Cosserat elasticity, gradient plasticity, and nonlocal elasticity have been recently popular, in part driven by the study of nano-scale phenomena. Nano-scale is not required for such effects to be substantial; it suffices that the largest structure size in the

material be non-negligible in comparison with representative size scales associated with gradients in applied fields of stress, electric polarization or other fields, holes, notches or cracks, or at least one structural component dimension. Nonlocal elasticity also provides additional freedom not present in the classical theory. The nonlocal theory incorporates long range interactions between particles in a continuum model. Such long range interactions occur between charged atoms or molecules in a solid. Long range forces may also be considered to propagate along fibers or laminae in a composite material [28] or in inclusions in random composites [29]. Nonlocality is often presented in a differential form that entails an approximation to the nonlocal integral [30]. Such a formulation introduces sensitivity to gradients of the stress or strain. Such gradient forms, termed nonlocal, have been presented [31] in the context of nano-scale systems. Cosserat elasticity reduces to a gradient form when $\kappa \to \infty$ or equivalently $N \to 1$, so there are points of contact between these formulations.

The toughness of foams [1] increases as the cell size ℓ_{cell}. Observe that toughness depends on structure size. This is in contrast with the theory of elasticity, which has no length scale within the theory. Cosserat elasticity is therefore considered to be pertinent to toughness.

5 Conclusions

Pure bending of a square cross section bar gives rise to a sigmoidal deformation of the lateral surfaces in addition to the usual tilt. This is shown both by a theoretical analysis of the bar as a isotropic Cosserat elastic solid, and by experiment on a bar of polymer foam. Observation of deformation of a single specimen reveals the presence of Cosserat elastic effects.

6 Acknowledgements

We gratefully acknowledge support of this research by the National Science Foundation via Grant CMMI-1361832.

References

[1] Gibson, L. J. and Ashby, M. F., 1997, *Cellular Solids*, Pergamon, Oxford; 2nd Ed., Cambridge.
[2] Cosserat, E. and Cosserat, F., 1909, *Theorie des Corps Deformables*, Hermann et Fils, Paris.
[3] Eringen, A.C., 1968, Theory of micropolar elasticity. In *Fracture* **1**, 621-729 (edited by H. Liebowitz), Academic Press.
[4] Hadjesfandiari, A. R. and Dargush, G. F., 2011, Couple stress theory for solids, Int. J. Solids, Structures **48**, pp. 2496-2510.
[5] Koiter, W. T., 1964, Couple-Stresses in the theory of elasticity, Parts I and II, Proc. Koninklijke Ned. Akad. Wetenshappen **67**, pp. 17-44.
[6] Lakes, R. S., 1986, Experimental microelasticity of two porous solids, Int. J. Solids and Structures, **22**, pp. 55-63.
[7] Anderson, W. B. and Lakes, R. S., 1994, Size effects due to Cosserat elasticity and surface damage in closed-cell polymethacrylimide foam, Journal of Materials Science, **29**, pp. 6413-6419.
[8] Spadoni, A. and Ruzzene, M., 2012, Elasto-static micropolar behavior of a chiral auxetic lattice, Journal of the Mechanics and Physics of Solids **60**, 156-171.
[9] Adomeit, G., 1967, Determination of elastic constants of a structured material, Mechanics of Generalized Continua, (Edited by Kröner, E.), IUTAM Symposium, Freudenstadt, Stuttgart. Springer, Berlin.
[10] Bigoni, D. and Drugan, W., 2007, Analytical Derivation of Cosserat Moduli via Homogenization of Heterogeneous Elastic Materials, J. Appl. Mech. **74**, pp. 741 - 753.
[11] Lakes, R. S., 1995, On the torsional properties of single osteons, J. Biomechanics, **28**, pp. 1409-1410.

[12] Gauthier, R. D. and W. E. Jahsman, 1975, A quest for micropolar elastic constants. J. Applied Mechanics, **42**, pp. 369-374.
[13] Mora, R. and Waas, A. M., 2000, Measurement of the Cosserat constant of circular cell polycarbonate honeycomb, Philosophical Magazine A **80**, pp. 1699-1713.
[14] Sikon, M., 2009, Theory and experimental verification of thermal stresses in Cosserat medium, Bulletin of the Polish Academy of Sciences: Technical Sciences, **57**(2), pp. 177 - 180.
[15] Krishna Reddy, G. V. and Venkatasubramanian, N. K., 1978, On the flexural rigidity of a micropolar elastic circular cylinder, J. Applied Mechanics **45**, pp. 429-431.
[16] Park, H. C. and R. S. Lakes, 1987, Torsion of a micropolar elastic prism of square cross section. Int. J. Solids, Structures, **23**, pp. 485-503.
[17] Park, H. C. and Lakes, R. S., 1986, Cosserat micromechanics of human bone: strain redistribution by a hydration-sensitive constituent, J. Biomechanics, **19**,pp. 385-397.
[18] Lakes, R. S., Gorman, D., and Bonfield, W., 1985, Holographic screening method for microelastic solids, J.Materials Science, **20**, pp. 2882-2888.
[19] Anderson, W. B., Lakes, R. S., and Smith, M. C., 1995, Holographic evaluation of warp in the torsion of a bar of cellular solid, Cellular Polymers, **14**, pp. 1-13.
[20] Iesan, D., 1971, On Saint Venant's problem in micropolar elasticity, Int. J. Engng Sci. **9**, pp. 879-888.
[21] Iesan, D., 1971, Bending of a micropolar elastic beam by terminal couples. Analele Stiintifice Universitatii Iasi Mathematica **17**, pp. 483-490.
[22] Reissner, E., 1968, On St. Venant flexure including couple stresses, PMM **32**, pp. 923-929.
[23] Park, S. K. and Gao, X. L., Bernoulli Euler beam model based on a modified couple stress theory, J. Micromech. Microeng **16**, pp. 2355-2359.
[24] Jemielita, G., 2006, Bending of a micropolar rectangular prism.I. Bull. Polish Acad. Sciences Tech. Sci. **32**, pp. 625-632 1984
[25] Foamade Industries, Auburn Hills, MI.
[26] Wang, Y. C., Lakes, R. S., and Butenhoff, A., 2001, Influence of cell size on re-entrant transformation of negative Poisson's ratio reticulated polyurethane foams, Cellular Polymers **20**, pp. 373-385.
[27] Tauchert, T., 1970, A lattice theory for representation of thermoelastic composite materials, Recent Advances in Engineering Science, **5**, pp. 325-345.
[28] Ilcewicz, L., Kennedy, T. C., and Shaar, C., 1985, Experimental application of a generalized continuum model to nondestructive testing, J. Materials Science Letters **4**, pp. 434-438.
[29] Drugan, W. J., 2003, Two Exact Micromechanics-Based Nonlocal Constitutive Equations for Random Linear Elastic Composite Materials, Journal of the Mechanics and Physics of Solids **51**, pp. 1745-1772.
[30] Eringen, A. C. 1983, On differential equations of nonlocal elasticity and solutions of screw dislocations and surface waves, J. Appl. Phys. **54**, pp. 4703-4710
[31] Peddieson, J. Buchanan, G. R., McNitt, R. P., 2003, Application of nonlocal continuum models to nanotechnology, Int. J. Engng. Sci. **41**, pp. 304-312.